



## The effect of turbulence model on predicting the development and progression of coronary artery atherosclerosis

Bahador Sharifzadeh<sup>a</sup>, Rasool Kalbasi<sup>a,\*</sup> and Mehdi Jahangiri<sup>b</sup>

<sup>a</sup>Department of mechanical engineering, Najafabad branch, Islamic Azad University, Najafabad, Iran.

<sup>b</sup>Department of mechanical engineering, Shahrekord branch, Islamic Azad University, Shahrekord, Iran

---

### Article info:

Type: Research  
Received: 02/01/2019  
Revised: 29/11/2019  
Accepted: 10/12/2019  
Online: 14/12/2019

### Keywords:

Oscillatory shear index,  
Time-averaged wall  
shear stress,  
Axial pressure drop,  
Shear stress.

### Abstract

A severe case of stenosis in coronary arteries results in turbulence in the blood flow which may lead to the formation or progression of atherosclerosis. This study investigated the turbulent blood flow in a coronary artery with rigid walls, as well as 80% single and double stenosis on blood flow. A finite element-based software package, ADINA 8.8, was employed to model the blood flow. The hemodynamic parameters of blood, such as the Oscillatory Shear Index (OSI) and the Mean Wall Shear Stress (Mean WSS) were obtained by both  $k - \epsilon$  and  $k - \omega$  turbulence models and then compared. According to the results, the negative pressure predicted by the  $k - \omega$  turbulence model was several times greater than that by the  $k - \epsilon$  turbulence model for both single and double stenosis. This, in turn, leads to the collapse of artery walls and irreparable injuries to the downstream extremity. Furthermore, the  $k - \omega$  model predicted a larger reverse flow region in the post-stenotic region. In other words, the  $k - \omega$  turbulence model predicts a larger part of the post-stenotic region to be prone to disease and the  $k - \epsilon$  turbulence model predicted a higher rate of plaque growth. Moreover, the  $k - \omega$  model predicted a much more intense reverse flow region than the  $k - \epsilon$  model, which itself can lead to blood pressure disease.

---

## 1. Introduction

Atherosclerosis is a blood artery disease caused by the deposition of lipids and low-density cholesterol in the inner walls of the arteries of medium to large diameters. As a result, fibrous-fatty plaques (atheroma) develop and grow gradually with aging or as a result of unhealthy habits, leading to artery stenosis or other complications. The narrowed lumen results in the perturbation of the blood flow, exacerbating or accelerating the progression of the disease.

Therefore, it is necessary to study the blood flow turbulence. Disease development and progression factors can be understood by studying blood flow patterns. Early studies on blood flow functions in the body return to the first findings in fluid dynamics. Fluid dynamics can be used to achieve hemodynamic parameters of blood [1, 2]. The hemodynamic parameters of blood can be in turn used for studying formation points, process, and timing of arterial occlusion [3]. Recently, several studies have been conducted on the blood flow

---

\*Corresponding author  
email address: jahangiri.m@iaushk.ac.ir

through an artery with a rigid wall. Some studies in this area are reviewed below:

Using the modified  $k-\varepsilon$  model, Ro et al. [4] conducted a numerical study on unsteady turbulent blood flow in a stenosed bifurcated artery with 75% constriction under periodic body acceleration. In this study, the blood was assumed to be a non-Newtonian fluid in a rigid wall artery. Applying different values of the periodic acceleration of the human body, it was found that this periodic acceleration leads to blood flow turbulence, affecting flow variables such as the volumetric flow rate and blood velocity. The wall shear stress (WSS) increased with increasing body acceleration.

Lantz et al. [5] conducted a numerical and experimental study to obtain turbulent kinetic energy in a rigid artery with stenosis using magnetic resonance imaging (MRI) and computational fluid dynamics (CFD) before and after cutter entry. They used Large Eddy Simulation (LES) model to simulate the blood flow. According to their results, the total turbulent kinetic energy decreased at the stenosis with increasing the blood flow rate and Reynolds number after the perturbation.

Li et al. [6] studied the pattern of blood flow in a bifurcated artery with a high degree of stenosis by *in vivo* magnetic resonance imaging and computational fluid dynamics at a Reynolds number of 200 to 900. The blood was assumed to be an incompressible Newtonian fluid flowing through a rigid-wall artery. Drawing on the transient flow model, in this study a Mean WSS peak was estimated at 73 Pa with high-WSS areas around the stenosis throat.

Hye and Paul [7] investigated rotational blood flow in rigid arteries with stenosis. Rotational and non-rotational blood flows were studied using 3D axially-symmetric stenosis models with 75% constriction using the standard transient  $k-\omega$  equation and the LES method at  $Re = 500, 1000, 1500, \text{ and } 2000$ . A steady, homogeneous, Newtonian, incompressible turbulent blood flow was assumed in the simulations. The results show that the spiral flow affects the turbulence kinetic energy in the post stenosis region. Other important results such as the wall pressure and shear stress remain almost unchanged by the spiral velocity. But the

presence of the upstream curved segment in artery moderately affects the results of the maximum pressure drop and wall shear stress.

Tabe et al. [8] simulated the transition of the laminar flow to a turbulent one to identify the relaminarization zones in a low Reynolds number blood flow through rigid arteries with severe single stenosis with 50% and 75% constrictions. Simulations were performed at Reynolds numbers of 500 to 2000 by using Fluent software. The  $k-\omega$  SST turbulence model was used to simulate the turbulent blood flow in turbulent regions. The flow was assumed to be Newtonian, steady and incompressible with axial symmetry. The results clearly showed that part by part simulation is an appropriate method for studying stenosed arteries. It can also be used to numerically simulate any stenosed conduit in different low Reynolds number applications where a laminar-to-turbulent transition and flow relaminarization take place. The flow changes from laminar to turbulent by increasing the degree of stenosis. The turbulent flow produces an eddy in the post-stenotic region. These eddies, in turn, exert reverse stresses to the inner layer of the artery causing damage to this layer. As a result of damages, macromolecules enter the inner layer and cause atherosclerosis. According to the literature, in reality, more than one stenosis forms in coronary arteries [9]. So far, few studies have been conducted on coronary arteries with double stenosis. The  $k-\varepsilon$  turbulence model has been extensively used to simulate the turbulent blood flow [3, 10-13]. Due to the inability of this model to simulate the post-stenotic eddies, the numerical results of this turbulence model are not well consistent with experimental results [10]. In this paper, the  $k-\omega$  turbulence model is used to simulate the turbulent blood flow. ADINA 8.8 finite element software was used to solve governing equations. Blood is assumed as a Newtonian incompressible fluid and the results of  $k-\varepsilon$  and  $k-\omega$  turbulence models are compared to predict atherosclerosis.

## 2. Governing equations

The turbulent, transient, and incompressible flow is governed by the Reynolds-averaged

Navier-stokes equation, which is as follows [14]:

$$\frac{D\bar{u}_i}{Dt} = -\frac{1}{\rho} \frac{\partial \bar{P}}{\partial x_i} + \frac{\partial}{\partial x_j} \left( \frac{\mu + \mu_T}{\rho} \left( \frac{\partial \bar{u}_i}{\partial x_j} + \frac{\partial \bar{u}_j}{\partial x_i} \right) \right) \quad (1)$$

The continuity equation is:

$$\frac{\partial \bar{u}_i}{\partial x_i} = 0 \quad (2)$$

In both  $k - \omega$  and  $k - \varepsilon$  turbulence models,  $\mu_T$  was calculated from Eqs. (3) and (4), respectively:

$$\mu_T = \rho \alpha \frac{k}{\omega} \quad (3)$$

$$\mu_T = \rho c_\mu \frac{k^2}{\varepsilon} \quad (4)$$

where  $c_\mu = 0.09$ .

In Eqs. (3) and (4),  $k$  represents the turbulence kinetic energy whereas  $\omega$  and  $\varepsilon$  are specific turbulence dissipation rates. Equations governing  $k$  and  $\omega$  are as follows:

$$\frac{\partial(y^a \rho k)}{\partial t} + \nabla \cdot [y^a (\rho v k - q_k)] = y^a G_k \quad (5)$$

$$\frac{\partial(y^a \rho \omega)}{\partial t} + \nabla \cdot [y^a (\rho v \omega - q_\omega)] = y^a G_\omega \quad (6)$$

$$q_\omega = \left( \mu_0 + \frac{\mu_T}{\sigma_\omega} \right) \nabla \omega \quad (7)$$

$$q_k = \left( \mu_0 + \frac{\mu_T}{\sigma_k} \right) \nabla k \quad (8)$$

$$G_\omega = \frac{\omega}{k} (2\alpha_\omega \mu_T D^2 - \beta_\omega \rho k \omega + \beta_\theta B) \quad (9)$$

$$G_k = 2\mu_T D^2 - \beta_K \rho k \omega + B \quad (10)$$

$$B = \left( \mu_0 + \frac{\mu_t}{\sigma_\theta} \right) \beta_g \cdot \nabla \theta \quad (11)$$

$$D = \sqrt{e_{ij} e_{ij}} \quad (12)$$

$$\beta = \frac{-(dp/d\theta)}{\rho} \quad (13)$$

where  $D$  indicates the deformation rate or the shear rate,  $\beta$  is the thermal expansion coefficient in the Boussinesq approximation,  $g$  represents the gravitational acceleration vector, and  $\theta$  is temperature in Kelvins.  $\alpha$ ,  $\alpha_\omega$ ,  $\beta_K$ ,  $\beta_\omega$ ,  $\sigma_\omega$ ,  $\sigma_\theta$ ,  $\sigma_\varepsilon$ , and  $\beta_\theta$  are empirical constants of the turbulence model. Where  $\alpha$ ,  $\alpha_\omega$ , and  $\beta_K$  were

derived from the  $k - \omega$  turbulence model at high Reynolds numbers. The constants corresponding to the  $k - \omega$  turbulence model at low Reynolds numbers are as follows:

$$\alpha = \alpha^h \frac{1/40 + R_k}{1 + R_k} \quad (14)$$

$$\alpha_\omega = \alpha_\omega^h \frac{1/10 + R_\omega}{1 + R_\omega} \alpha^{-1} \quad (15)$$

$$\beta_k = \beta_k^h \frac{5/18 + R_\beta}{1 + R_\beta} \quad (16)$$

where the superscript  $h$  indicates the parameter was determined at a large Reynolds number.

$$R_k = \frac{R_t}{6} \quad (17)$$

$$R_\omega = \frac{R_t}{2.7} \quad (18)$$

$$R_\beta = \left( \frac{R_t}{8} \right)^4 \quad (19)$$

$$R_t = \rho \frac{k}{\mu_0 \omega} \quad (20)$$

The empirical constants of the  $k - \omega$  turbulence model are given in Table 1.

Equations governing  $k$  and  $\varepsilon$  are as follows:

$$\frac{\partial(y^a \rho k)}{\partial t} + \nabla \cdot [y^a (\rho v k - q_k)] = y^a S_k \quad (21)$$

$$\frac{\partial(y^a \rho \varepsilon)}{\partial t} + \nabla \cdot [y^a (\rho v \varepsilon - q_\varepsilon)] = y^a S_\varepsilon \quad (22)$$

$$q_k = \left( \mu_0 + \frac{\mu_T}{\sigma_k} \right) \nabla k \quad (23)$$

$$q_\varepsilon = \left( \mu_0 + \frac{\mu_T}{\sigma_\varepsilon} \right) \nabla \varepsilon \quad (24)$$

$$S_k = 2\mu_T D^2 - \rho \varepsilon + B \quad (25)$$

$$S_\varepsilon = \frac{\varepsilon}{k} (2c_1 \mu_T D^2 - c_2 \rho \varepsilon + c_1(1 - c_3)B) \quad (26)$$

$$B = \left( \mu_0 + \frac{\mu_t}{\sigma_\theta} \right) \beta_g \cdot \nabla \theta \quad (27)$$

$$D = \sqrt{e_{ij} e_{ij}} \quad (28)$$

where the empirical constants  $c_1$ ,  $c_2$ ,  $c_3$ ,  $\sigma_k$ ,  $\sigma_\varepsilon$ , and  $\sigma_\theta$  are 1.44, 1.82, 0.8, 1, 1.3, and 0.9, respectively.

**Table 1:** The empirical constants of the turbulence model [15].

$\alpha = 1$	$\alpha_\omega = 0.555$	$\beta_k = 0.09$	$\beta_\omega = 0.075$
$\sigma_\omega = 2$	$\beta_\theta = 0.712$	$\sigma_\theta = 1$	$\sigma_k = 2$

In the relations presented for the two turbulence models,  $v$  represents the vertical component of the velocity vector, and  $y$  is the second coordinate of the position vector.  $a$  is zero for two- and three-dimensional flows and 1 for the axisymmetric one.

Turbulent boundary conditions were assumed at the fluid inlet. The turbulence intensity ( $i$ ) and the turbulence length scale ( $l$ ) are calculated using the following relations:

$$i = 0.16 \left( \frac{\rho U_0 D}{\mu} \right)^{-\frac{1}{8}} \quad (29)$$

$$l = 0.07L = 0.07D \quad (30)$$

In Eqs. (29) and (30),  $D$  is the artery diameter,  $U_0$  represents the average fluid velocity,  $\mu$  indicates the fluid viscosity, and  $\rho$  is the fluid density.

### 3. Solution validation

To ensure the reliability of the numerical results, they were compared with the experimental data reported by Ahmed and Giddens [16], the numerical data presented by Banks et al. [12], and Jahangiri et al. [3]. As evident from Fig. 1, the numerical results of the present study are much more consistent with the experimental data of Ahmed and Giddens [16]-especially near the walls-relative to other numerical studies [3, 12]. The results indicate that moving further away from the throat of the stenosis, the presented model exhibits a better match with experimental data in comparison with similar works. The results are consistent with the claim that the advantage of  $k-\omega$  model over  $k-\epsilon$  is its improved function at boundary layers under adverse pressure gradient [17].

### 4. Numerical methods

An artery model with axially-symmetric stenosis and rigid walls was used in this study.

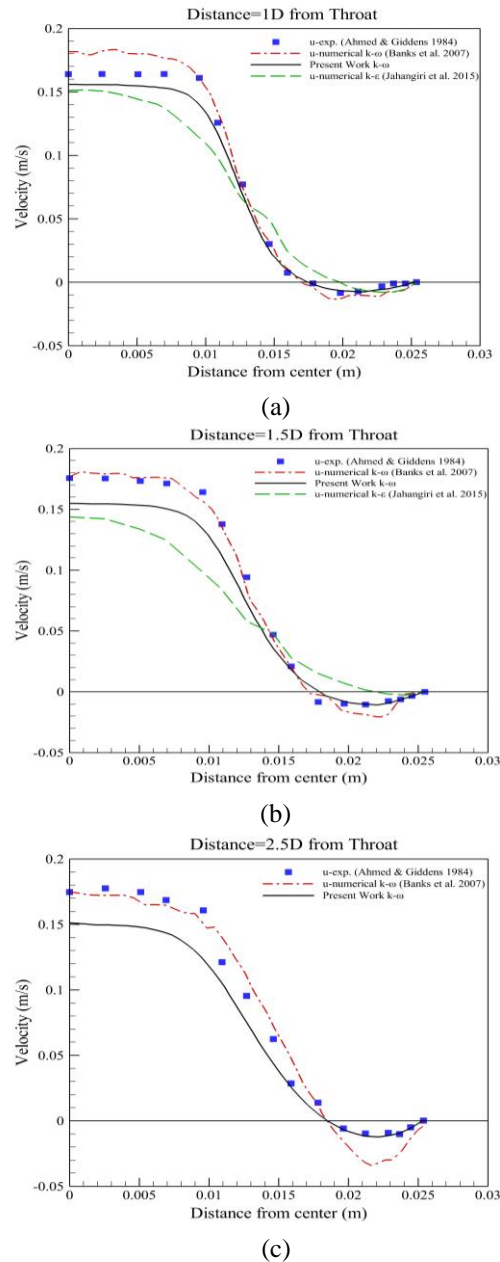


**Fig. 1.** Velocity profile at different intervals. (a) 1D from the stenosis throat, (b) 1.5D from the stenosis throat, and (c) 2.5D from the stenosis throat.

The onset of flow turbulence has been shown to be at stenosis with a constriction of over 80% [3]. So, a constant 80% stenosis was assumed in this study. The computational domain and its dimensions are illustrated in Fig. 2. The arterial equation in the stenosis region is as follows [18]:

$$\frac{R(z)}{R_0} = 1 - \left( \frac{R_0 - R_{0,t}}{2R_0} \right) \times \left( 1 + \cos \frac{2\pi(z - z_m)}{L_{st}} \right) \quad (31)$$

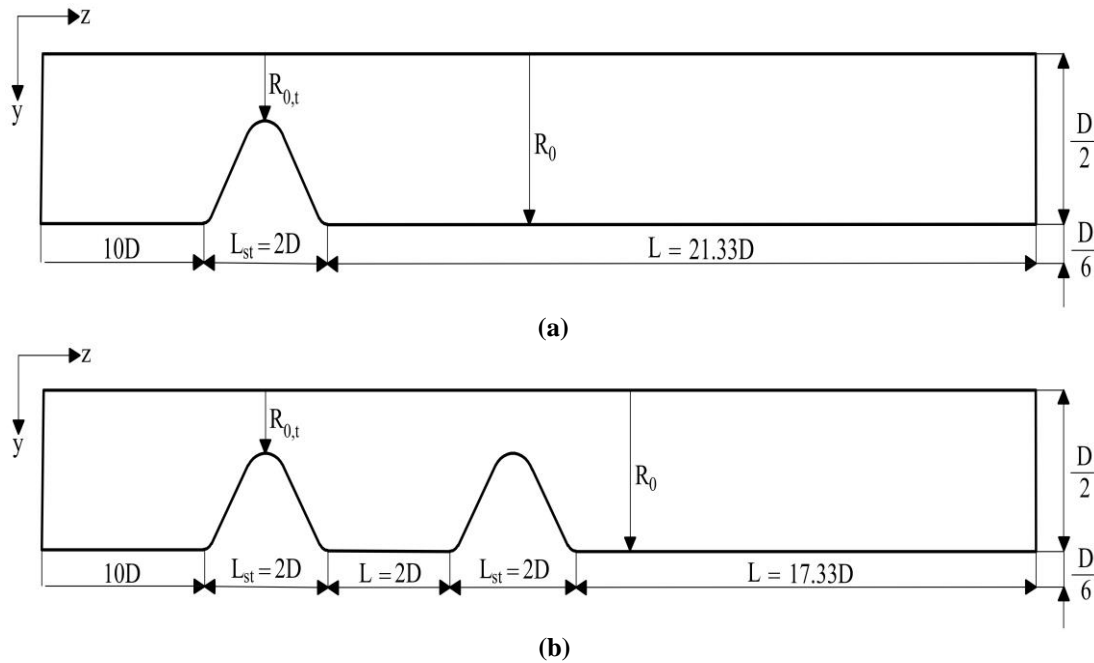


Fig. 2. Computational domain for the arteries with: (a) single stenosis and (b) double stenosis.

Blood was considered in the simulations as a fluid with a viscosity of 0.0033 Pa.s and a density of 1050 kg/m<sup>3</sup>. The average velocity profile applied to the fluid inlet for a right coronary artery (Fig. 3) has been provided by Zeng et al. [19]. To avoid variation of solutions, three velocity pulses were applied at the fluid inlet and the results were computed in the third pulse [20-23]. To achieve results independent of grid and time step for determining the most accurate solutions and minimizing computer runtime, the independence of solutions from the number of computational grids and time step was examined.

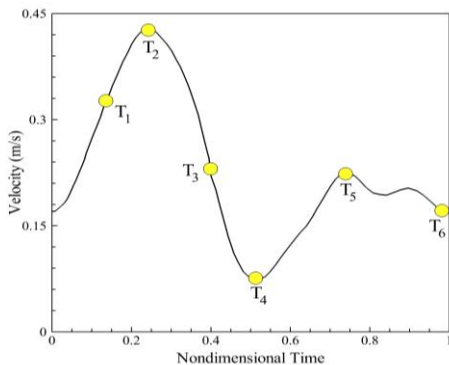


Fig. 3. Velocity pulse applied to the fluid inlet [19].

To ensure the grid independence of the results, the axial velocity profile is demonstrated in Fig. 4 at a distance of one diameter (1D) from the stenosis throat for three different grid modes. As evident, the results obtained from a grid with 10,200 cells are very close to those obtained from 15,300 cells. So the mesh with 10,200 cells was used to reduce the computational cost and time. Simulations were performed on a computer with a 3.5 GHz processor and 16 GB of memory.

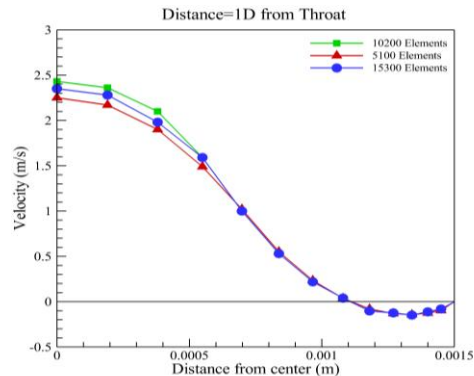


Fig. 4. Axial velocity profile at a distance of 1D from the stenosis throat.

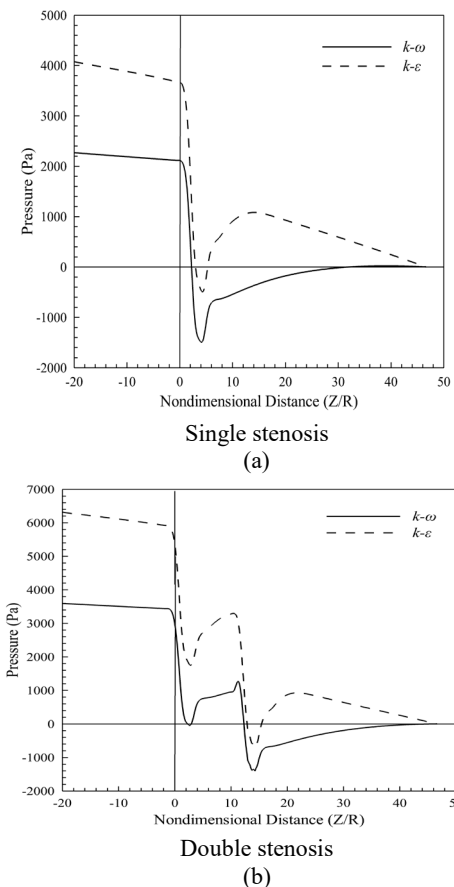
### 5. Results and discussion

Blood pressure difference along the coronary artery is an important cause of atherosclerosis and intimal hyperplasia [24]. Fig. 5 compares axial pressure drop across the artery at the time of maximum flow velocity (the third pulse at 3.25 s) for arteries with single and double stenosis obtained from the  $k-\epsilon$  and  $k-\omega$  turbulence models.

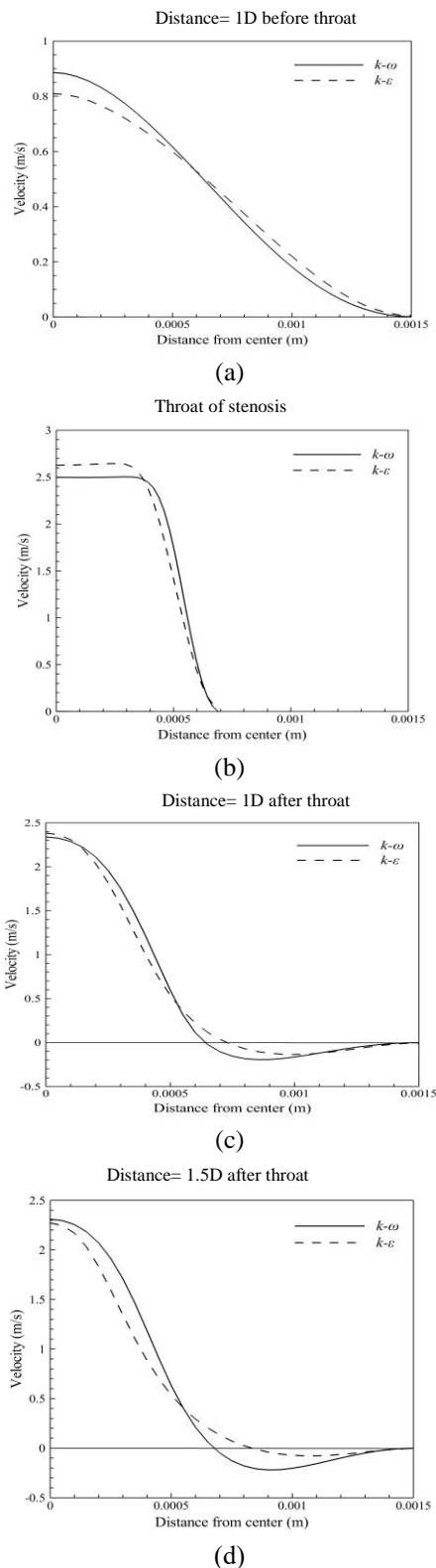
As evident from Fig. 5, the  $k-\epsilon$  turbulence model predicts a higher pressure drop than the  $k-\omega$  turbulence model. Furthermore, the difference between the two turbulence models is minimal at the entrance to the stenosis where the fluid accelerates. The pressure is higher in double stenosis than that in single stenosis. Therefore, the upstream pressure reaches a critical value earlier in double stenosis as compared with single stenosis leading to a non-physiological increase in the upstream pressure and systemic pressure. Notably, the  $k-\omega$  turbulence model predicts the reverse pressure several times larger than the one predicted by the  $k-\epsilon$  model. In the most critical conditions, reverse pressure may lead to the collapse of the vascular wall and blood flow occlusion [25] with irreparable damages to lower extremity. The largest reverse pressure is observed in the single stenosis throat [24] or in the second stenosis throat of the double-stenosed artery. In this region, the flow path becomes narrower and the risk of occlusion increases. In some cases, the vessels collapse immediately following a stenosis [26, 27]. The collapse of the vascular wall in negative pressure (reverse) can be related to a considerable reduction of the vessel wall elasticity [28]. In addition, pressure loading fluctuations may lead to fatigue failure of the plaque [29, 30]. The collapse of the vessel leads to hemodynamic changes that may lead to angina, myocardial ischemia, cardiac arrhythmias, syncope, or even death [31, 32]. Therefore, it is necessary to recognize and investigate the collapse of vessels that leads to vascular dysfunctions.

Fig. 6 shows velocity profiles for two turbulence models at the time of maximum flow velocity (the third pulse at 3.25 s) at different distances from the throat for a single-stenosed artery.

It is evident that the  $k-\epsilon$  turbulence model predicts a smaller reverse flow region. In other words, the  $k-\omega$  turbulence model predicts a wider area to be prone to disease in the post-stenotic region, whereas a larger plaque growth rate is obtained using the  $k-\epsilon$  turbulence model [11]. Another important feature of Fig. 6 is that both the length of the reverse flow area and its intensity are less in the  $k-\epsilon$  model than the  $k-\omega$  model. Given the fact that the maximum negative velocity is related to pulmonary hypertension [33], the  $k-\omega$  model is more accurate in estimating the risk of this disease. The blood flow velocity is of great importance because the thrombosis growth rate is affected by blood flow velocity [34, 35]. It has been found that the oxygen pressure in living tissues is dependent on the blood flow velocity [36]. In addition, the blood flow velocity directly affects thrombosis due to platelet aggregation [37].



**Fig. 5.** Comparison of the axial pressure drop in (a) single and (b) double stenosis obtained from two turbulence models.



**Fig. 6.** Velocity profile for single stenosis at the time of maximum flow velocity.

According to the above diagrams, the velocity profile is steeper in the  $k-\epsilon$  turbulence model than in the  $k-\omega$  model. Before and after the throat, the  $k-\omega$  turbulence model shows a higher maximum axial velocity. However, the  $k-\epsilon$  turbulence model predicts a higher maximum axial velocity in the throat. According to the velocity profile in the stenosis throat, the maximum velocity is much higher than 1 m/s (in the center of artery) beyond a natural biological state and may cause disturbances in the circulatory system [35]. Also the maximum velocity decreases at the end of stenosis in comparison with the throat.

Fig. 7. shows velocity profiles for two turbulence models at the time of maximum flow velocity (the third pulse at 3.25 s) at different distances from the first and second throats for a double-stenosed artery. The velocity profiles for double stenosis are similar to those for single stenosis with this difference that the  $k-\omega$  turbulence model predicts the maximum velocity in the second throat. Moreover, the difference between the two turbulence models is maximized in between the two stenosis. A more important result of the  $k-\omega$  model that is unprecedented in previous studies [3, 10, 13], is that the  $k-\epsilon$  model was not capable of showing the reverse flow between two stenosis. One can see from the results in that the entire distance between the two stenosis is affected by the reverse flow. In other words, this region is very susceptible to the accumulation of fat particles and their penetration into the vascular wall and formation of a new stenosis between two stenosis. As found in other research works [38], the reverse flow has a fundamental role in stenosis formation. Perturbations at arterial walls and monocyte and LDL movement below the endothelial space is referred to as atherogenesis [39] and leads to atheroma formation [40].

The importance of studying stenosis at distances less than 5D apart lies in the different effects of dual and single stenosis [41]. Furthermore, it must be noted that consecutive stenosis has been associated with pulmonary hypertension [42].

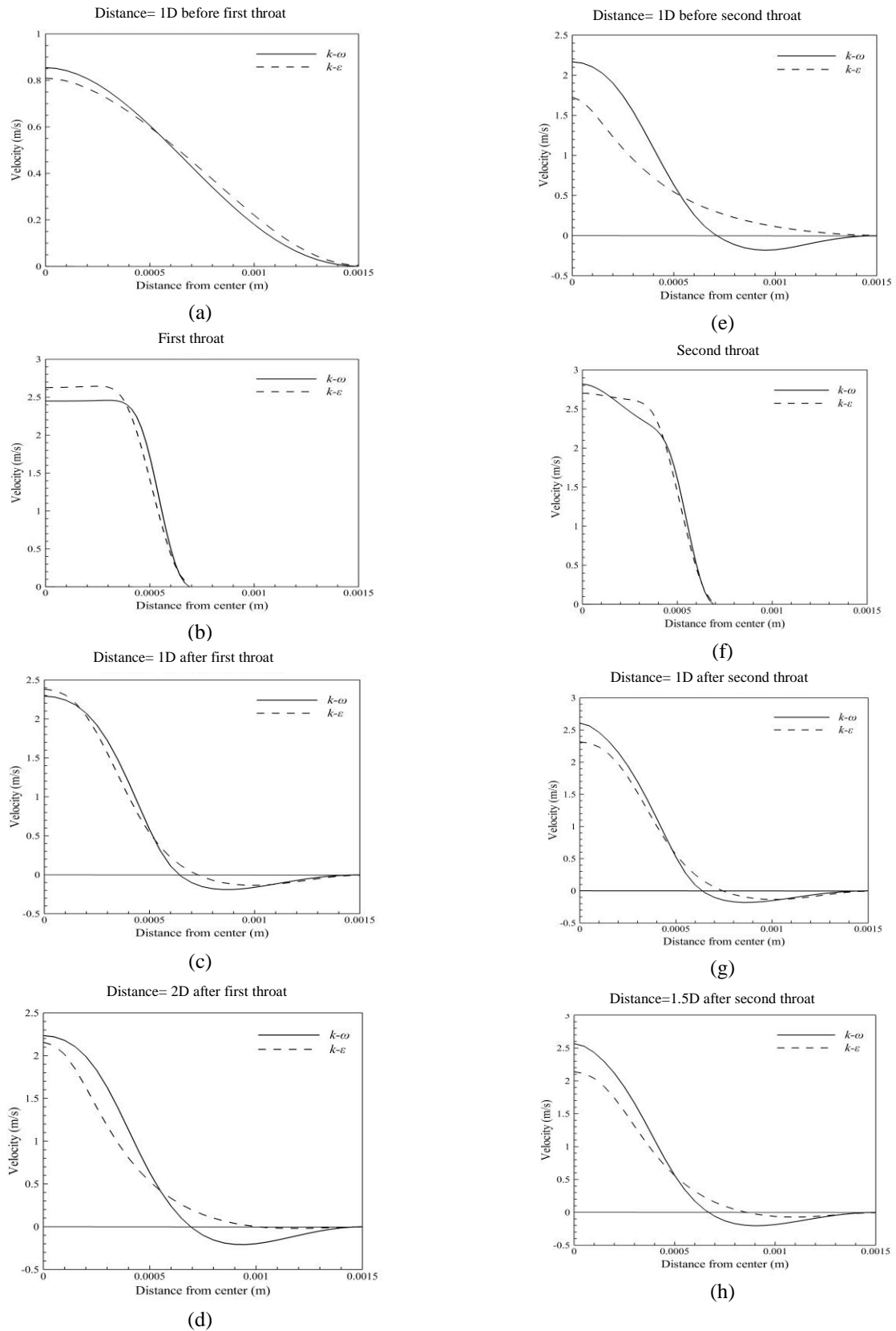


Fig. 7. Velocity profile for double stenosis at the time of maximum flow velocity.

Mean Wall Shear Stress (WSS) and oscillatory shear index (OSI) are two hemodynamic parameters of blood that play a key role in predicting the location and development of vascular diseases. The direction of the wall shear stress has been reported to be vital in controlling endothelial mechanotransduction and downstream signaling pathways [43]. Further, it has been discussed that the direction of the hemodynamic stress can disrupt the balance of pro- and anti-atherosclerotic signals in endothelial cells.

Fig. 8-9 compare OSI and Mean WSS hemodynamic parameters obtained from the two turbulence models for arteries with single and double stenosis.

The OSI is a mechanical parameter for fluctuating flow and indicates the deviation of WSS from the dominant direction of blood flow during a cardiac period. The OSI is variable from zero (no change in the WSS direction) to 0.5 (for a 180° change in the direction of WSS) [44]. Despite the dependence of the plaque formation mechanism to a great many biological parameters, OSI factor is a useful measure as regards oscillatory blood flow [3, 13, 45]. According to experimental results, the maximum OSI takes place at plaque formation site [46-49].

The OSI and the Mean WSS are obtained from Eqs. (32) and (33), respectively [50]:

$$OSI = 0.5 \times \left( 1 - \frac{\left| \int_0^T \tau_w dt \right|}{\int_0^T |\tau_w| dt} \right) \quad (32)$$

$$MeanWSS = \frac{1}{T} \int_0^T \tau_w dt \quad (33)$$

where T is the period of a cardiac cycle and  $\tau_w$  is the WSS vector. Fig. 8-9 compares two hemodynamic parameters obtained from the two turbulence models for arteries with single and double stenosis.

Two peaks appear in the OSI diagrams in the case of a single stenosis, whereas four are seen in those corresponding to a double stenosis. The first peak in the single stenosis represents the flow separation point and the second peak indicates the reattachment point. The first peak

in the double stenosis represents the flow separation point whereas the second peak shows the reattachment point in the first post-stenotic region. The third peak represents the separation point and the fourth peak shows the reattachment point in the second post-stenotic region. In other words, the distance between the first and second peaks as well as the third and fourth peaks represents the length of the reverse flow regions.

According to the OSI diagrams in Fig. 8, the separation points predicted by two turbulence models are matched. While predicting a smaller reverse flow region, the k-ε turbulence model locates the reattachment point at a small distance in the post-stenotic region. In contrast, the k-ω turbulence model predicts the reattachment of the reverse flow at a distance far from the stenosis. According to the OSI diagrams in Fig. 8, by changing the single stenosis to double stenosis in the k-ω turbulence model, the length of the separation area after the first stenosis decreases and a larger separation zone than single stenosis is formed in the second post-stenotic region.

The mean WSS clearly shows that the k-ε model estimates a larger maximum WSS while underestimates the reverse flow region. In other words, the k-ω model has a lower damage to the plaque and the risk of its rupture compared to the k-ε model. Rather, it predicts the formation of a new stenosis behind the previous one. This is of great importance because the reduced shear stress on arterial walls is the most important parameter in determining the progression of atherosclerosis [51, 52].

Under a wall shear stress of over 1 Pa, endothelial cells tend to stretch along the flow direction while taking a round shape with no regularities under stresses of below 0.4 Pa. The round cells in stagnant areas allow a higher infiltration of haematogenous cells into the walls of blood vessels, causing artery diseases [35]. Based on these points, the k-ε model predicted the round cells to form closer to the stenosis compared to the k-ω model. It has been stated that blood flow-induced shear stress plays a key role in the pathogenesis of some cardiovascular diseases [53].

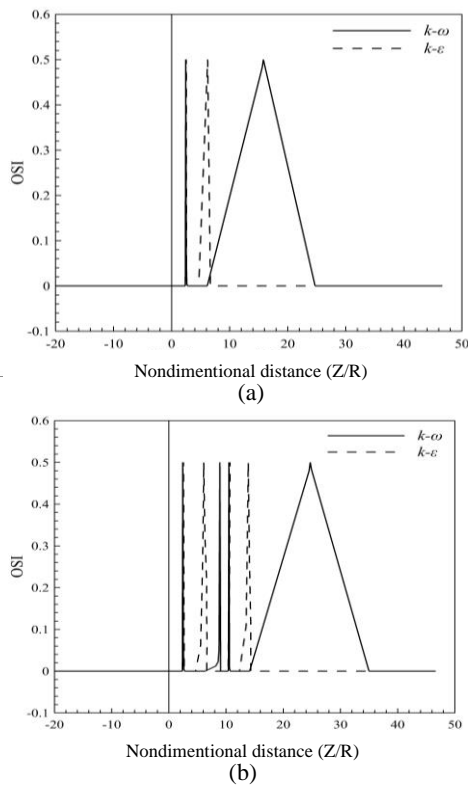


**Fig. 8.** OSI comparison of the two turbulence models for arteries with (a) single and (b) double stenosis.

Severe stenosis (above 75%) can lead to the separation of the blood flow and create a sizeable reverse flow region downstream of the stenosis, which can have a direct contribution to the development of the disease.

Considering the relationship between blood flow-induced stresses and the pathogenesis of atherosclerosis and thrombosis [24], the contours of the flow separation and reverse flow regions were examined in Figs. 10-17.

The reverse flow and velocity contours are presented for  $k-\omega$  and  $k-\epsilon$  turbulence models in the following.

Figs. 10-11 show reverse flow contours obtained from the two turbulence models for a single-stenosed artery at the maximum and minimum flow velocities at  $T_2$  and  $T_4$ , respectively. According to the reverse flow contours for the single stenosis, the length of the reverse flow region at the maximum and minimum velocities is predicted much larger by  $k-\omega$  model. In the  $k-\epsilon$  turbulence model, the maximum reverse flow takes place near the stenosis which exacerbates stenosis. However,

the results of the  $k-\omega$  model indicate a new stenosis behind the previous one.

Figs. 12-13 show the velocity contours obtained from the two turbulence models for a single-stenosed artery at  $T_2$  (maximum flow velocity). It is evident that the maximum velocity in both turbulence models takes place at the stenosis throat on the artery centerline. By narrowing the duct, the flow is accelerated and moves toward the axis. In addition, as the velocity reaches its maximum at the stenosis throat, the pressure is minimized. The maximum velocity is higher in the  $k-\epsilon$  model.

Figs. 14-15 show reverse flow contours obtained from the two turbulence models for a double-stenosed artery at the maximum and minimum velocities at  $T_2$  and  $T_4$ , respectively. Similar to the single stenosis, the  $k-\omega$  model predicts a much larger length and intensity for the post-stenotic reverse flow region.

According to the results of the  $k-\epsilon$  model, a small zone between the two stenosis is affected by the reverse flow. In other words, the  $k-\omega$  model shows that the region between the two stenosis is at risk of atherosclerosis at the maximum and minimum flow velocities.

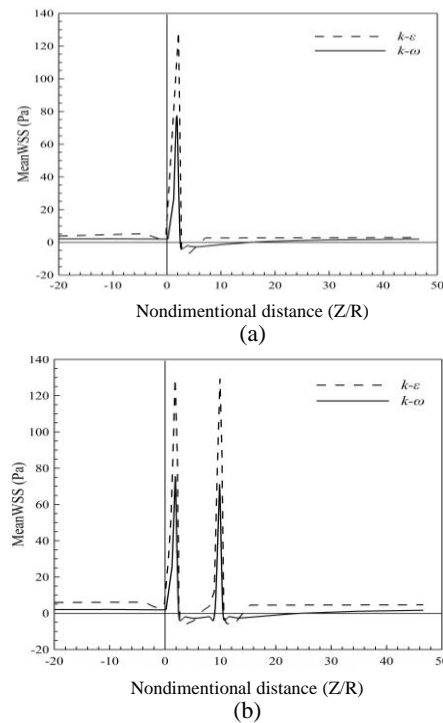


**Fig. 9.** Mean WSS comparison of two turbulence models for arteries with (a) single and (b) double stenosis.

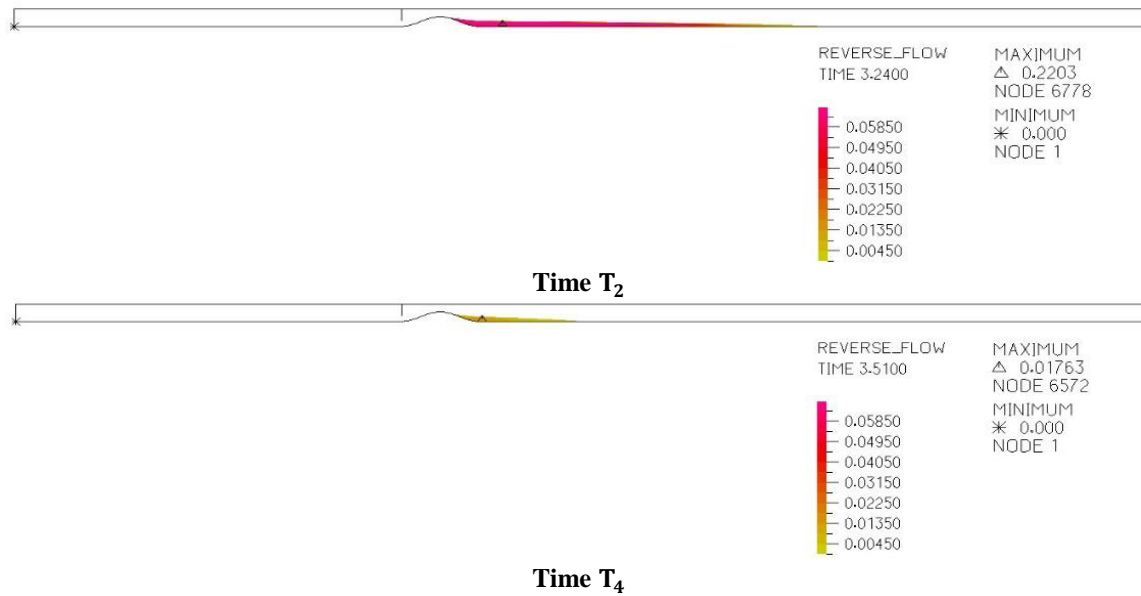


Fig. 10. Reverse flow contour for a single-stenosed artery using the k- $\omega$  turbulence model.

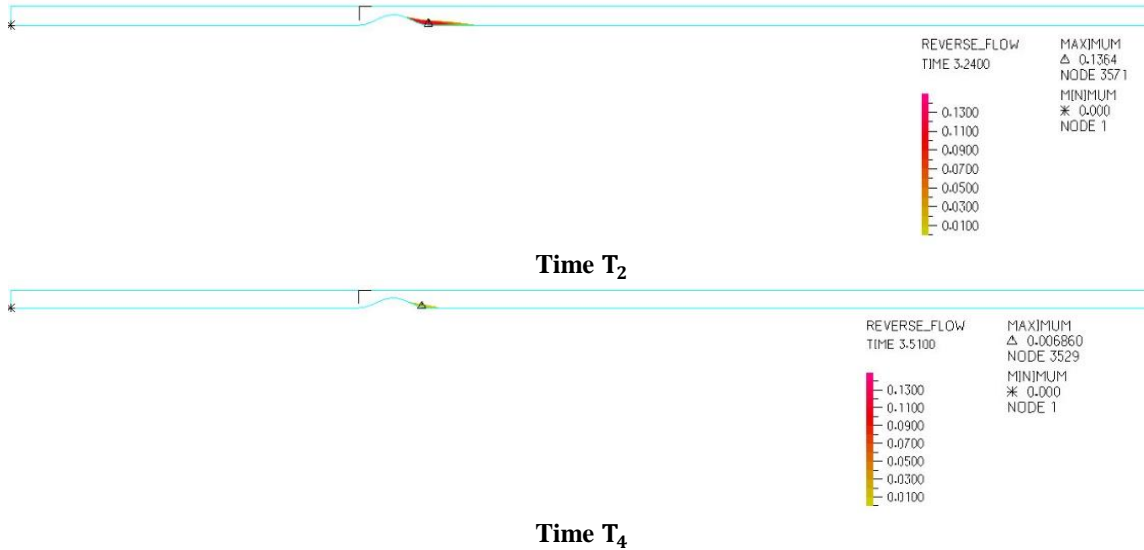


Fig. 11. Reverse flow contour for a single-stenosed artery using the k- $\epsilon$  turbulence model.

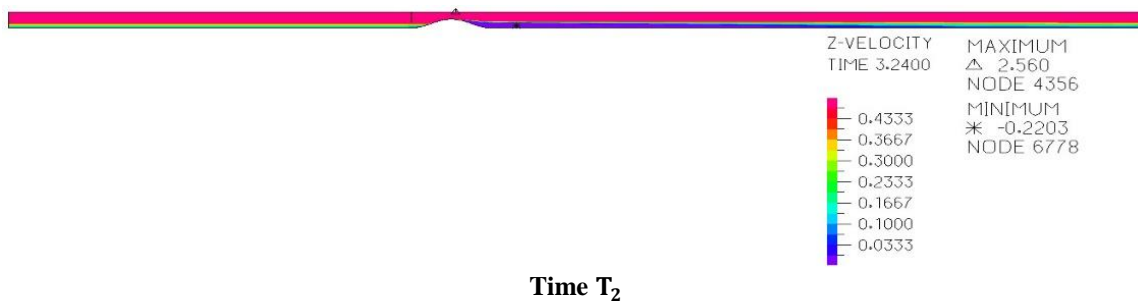


Fig. 12. Velocity contour obtained from the k- $\omega$  turbulence model for a single-stenosed artery.

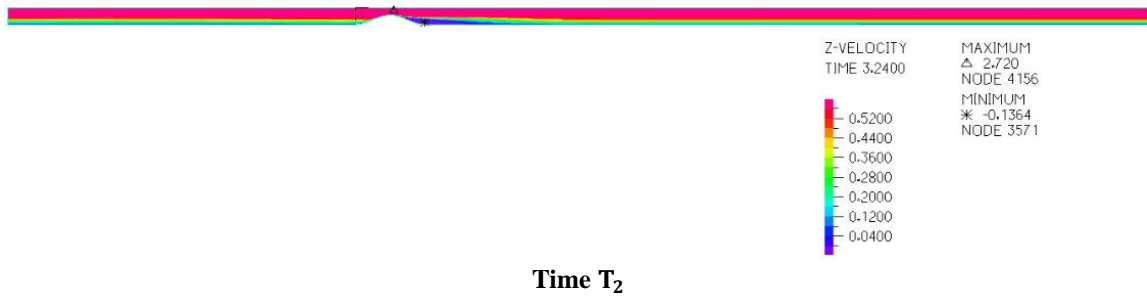


Fig. 13. Velocity contour obtained from the k-ε turbulence model for a single-stenosed artery.

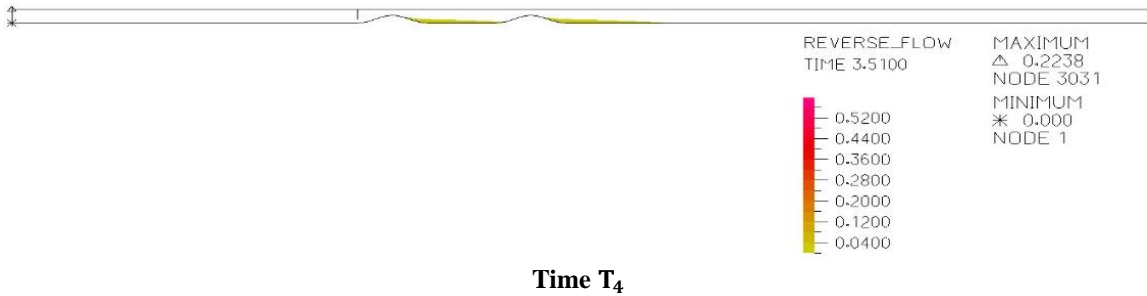
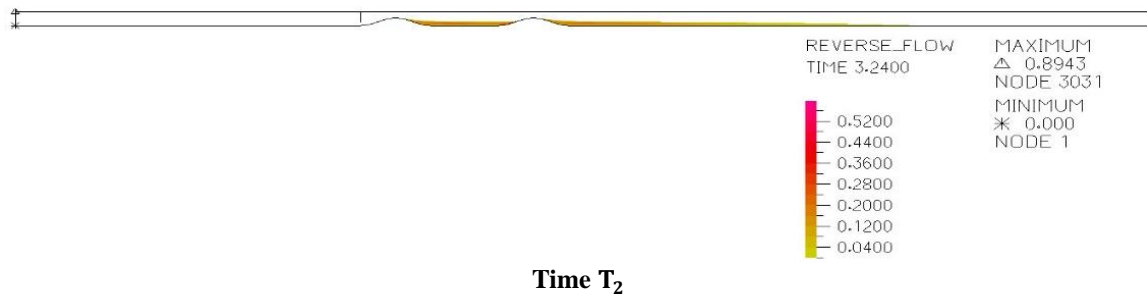


Fig. 14. Reverse flow contours for a double-stenosed artery obtained from k-ω turbulence model.

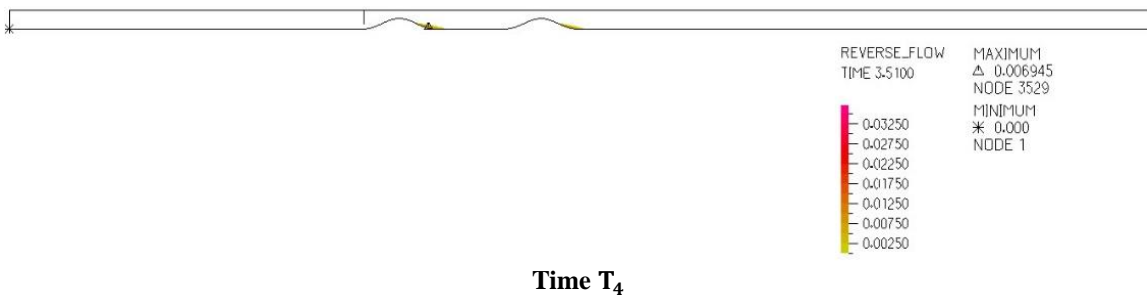
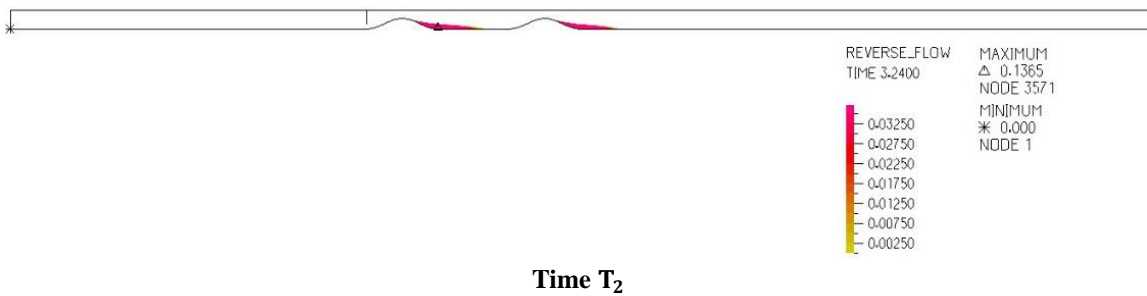
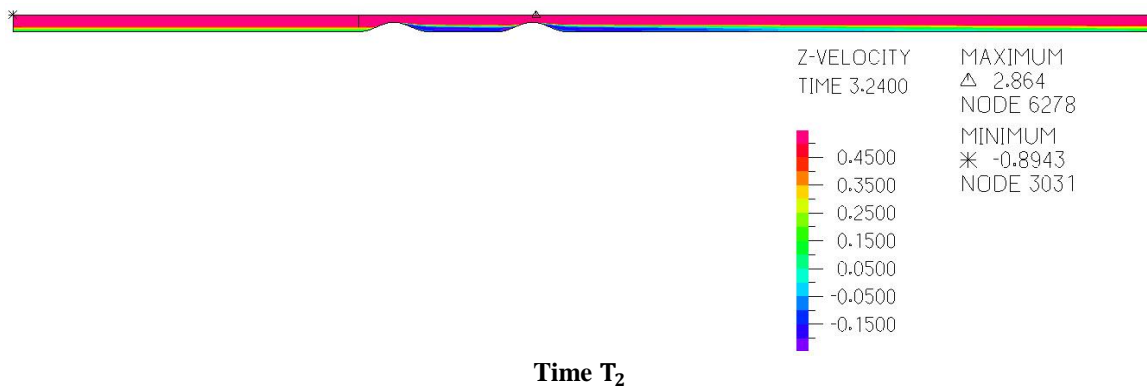
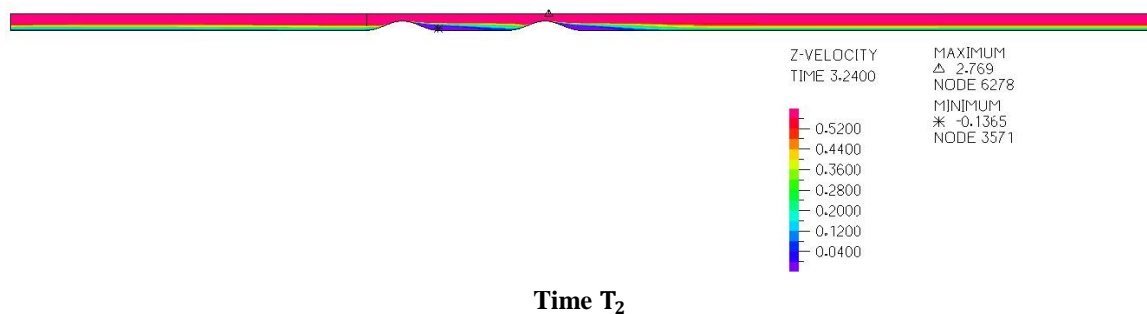


Fig. 15. Reverse flow contours for a double-stenosed artery obtained from k-ε turbulence model.



**Fig. 16.** Velocity contour obtained from the k- $\omega$  turbulence model for a double-stenosed artery.



**Fig. 17.** Velocity contour obtained from the k- $\epsilon$  turbulence model for a double-stenosed artery.

The velocity contours obtained from the two turbulence models are illustrated in Figs. 16-17 for a double-stenosed artery at T<sub>2</sub> (maximum flow velocity). As evident from the figures, the maximum velocity takes place at the second stenosis throat where the blood-passing through the first stenosis-flows toward the artery centerline. Due to the short distance between the stenosis, blood does not have enough time to go

#### 4. Conclusions

The turbulent blood flow in a rigid-wall coronary artery with single and double stenosis was investigated. ADINA 8.8 finite element software was used to model the blood flow. The results can be expressed as follows:

- The k- $\omega$  turbulence model predicted the negative pressure several times greater than the k- $\epsilon$  turbulence model in both single and double stenosis modes.
- The k- $\omega$  model predicted a much lengthier post-stenotic reverse flow region. In other words, the k- $\omega$  turbulence model predicts a

back to the wall as found in the results of other studies in this area [3].

It has been argued that higher blood velocity promotes eddies and fluctuations, increasing turbulence shear stresses to the point of exceeding threshold conditions and increasing the risk of hemolysis (rupturing of RBC membranes) and the activation of platelets [54, 55], which points to another area of interest in the study of blood velocity.

larger area to be prone to the disease in the post-stenotic region.

- The plaque growth rate was higher in the k- $\epsilon$  turbulence model in comparison to k- $\omega$  model.
- The intensity of the reverse flow region predicted by the k- $\omega$  model was much greater than the k- $\epsilon$  model causing pulmonary hypertension.
- A higher maximum blood flow velocity was predicted by the k- $\omega$  model at most points.
- Given the direct impact of the blood velocity on the growth rate of thrombosis, the turbulence model types play an important role in predicting the development and progression of atherosclerosis.

## References

- [1] S. Fazli, E. Shirani and M. R. Sadeghi, "Numerical Simulation of LDL Mass Transfer in a Common Carotid Artery under Pulsatile Flows", *Journal of Biomechanics*, Vol. 44, pp. 68-76, (2011).
- [2] A. Razavi, E. Shirani and M. R. Sadeghi, "Numerical Simulation of Blood Pulsatile Flow in a Stenosed Carotid Artery Using Different Rheological Models", *Journal of Biomechanics*, Vol. 44, pp. 2021-2030, (2011).
- [3] M. Jahangiri, M. Saghafian and M. R. Sadeghi, "Numerical simulation of hemodynamic parameters of turbulent and pulsatile blood flow in flexible artery with single and double stenosis", *Journal of Mechanical Science and Technology*, Vol. 29, No. 8, pp. 3549-3560, (2015).
- [4] K. C. Ro and S. R. Hong, "Numerical study on turbulent blood flow in a stenosed artery bifurcation under periodic body acceleration using a modified k- $\epsilon$  model", *Korea-Australia Rheology Journal*, Vol. 22, No. 2, pp. 129-139, (2010).
- [5] J. Lantz, T. Ebbers, J. Engvall and M. Karlsson, "Numerical and experimental assessment of turbulent kinetic energy in an aortic coarctation", *Journal of biomechanics*, Vol. 46, No. 11, pp. 1851-1858, (2013).
- [6] Z. Y. Li, F. P. Tan, G. Soloperto, N. B. Wood, X. Y. Xu and J. H. Gillard, "Flow pattern analysis in a highly stenotic patient-specific carotid bifurcation model using a turbulence model", *Computer methods in biomechanics and biomedical engineering*, Vol. 18, No. 10, pp. 1099-1107, (2015).
- [7] M. A. Hye and M. C. Paul, "A computational study on spiral blood flow in stenosed arteries with and without an upstream curved section", *Applied Mathematical Modelling*, Vol. 39, No. 16, pp. 4746-4766, (2015).
- [8] R. Tabe, F. Ghalichi, S. Hossainpour and K. Ghasemzadeh, "Laminar-to-turbulence and relaminarization zones detection by simulation of low Reynolds number turbulent blood flow in large stenosed arteries", *Bio-medical materials and engineering*, Vol. 27, No. 2-3, pp. 119-129, (2016).
- [9] M. R. Sadeghi, *Numerical simulation of blood flow in vessels with arterial stenosis considering fluid structure interaction*, PhD Thesis, Isfahan University of technology, (2013).
- [10] M. Jahangiri, M. Saghafian and M. R. Sadeghi, "Numerical study of hemodynamic parameters in pulsatile turbulent blood flow in flexible artery with stenosis". *Annual International Conference on Mechanical Engineering-ISME*, Shahid Chamran University, Ahvaz, Iran, pp. 1-5, (2014).
- [11] S. S. Varghese and S. H. Frankel, "Numerical modeling of pulsatile turbulent flow in stenotic vessels", *Journal of biomechanical engineering*, Vol. 125, No. 4, pp. 445-460, (2003).
- [12] J. Banks and N. W. Bressloff, "Turbulence modeling in three-dimensional stenosed arterial bifurcations", *Journal of biomechanical engineering*, Vol. 129, No. 1, pp. 40-50, (2007).
- [13] M. Jahangiri, M. Saghafian and M. R. Sadeghi, "Numerical study of turbulent pulsatile blood flow through stenosed artery using fluid-solid interaction", *Computational and mathematical methods in medicine*, Vol. 2015, Article ID 515613, pp. 1-10, (2015).
- [14] Theory and modeling guide, Volume III: ADINA CFD & FSI, *Help of ADINA software*, (2011).
- [15] ADINA User Manuals, ADINA R&D, Inc, (2011).
- [16] S. A. Ahmed and D. P. Giddens, "Pulsatile poststenotic flow studies with laser Doppler anemometry" *Journal of biomechanics*, Vol. 17, No. 9, pp. 695-705, (1984).
- [17] F. Khalili, P. Gamage and H. A. Mansy, "Verification of Turbulence Models for Flow in a Constricted Pipe at Low

- Reynolds Number”, *arXiv preprint*, arXiv: 1803.04313, pp. 1-10, (2018).
- [18] M. R. Sadeghi, E. Shirani, M. Tafazzoli-Shadpour and M. Samaee, “The effects of stenosis severity on the hemodynamic parameters-assessment of the correlation between stress phase angle and wall shear stress”, *Journal of biomechanics*, Vol. 44, No. 15, pp. 2614-2626, (2011).
- [19] D. Zeng, E. Boutsianis, M. Ammann, K. Boomsma, S Wildermuth and D Poulidakos, “A study on the compliance of a right coronary artery and its impact on wall shear stress”, *Journal of biomechanical engineering*, Vol. 130, No. 4, Article ID 041014, pp. 1-11, (2008).
- [20] M. Jahangiri, A. Haghani, R. Ghaderi and S. M. Harat, “Effect of Non-Newtonian Models on Blood Flow in Artery with Different Consecutive Stenosis”, *International Journal of Advanced Design & Manufacturing Technology*, Vol. 11, No. 1, pp. 79-86, (2018).
- [21] M. Jahangiri, M. Saghafian and M. R. Sadeghi, “Effects of non-Newtonian behavior of blood on wall shear stress in an elastic vessel with simple and consecutive stenosis”, *Biomedical and Pharmacology Journal*, Vol. 8, No. 1, pp. 123-131, (2015).
- [22] M. Jahangiri, M. Saghafian and M. R. Sadeghi, “Effect of six non-Newtonian viscosity models on hemodynamic parameters of pulsatile blood flow in stenosed artery”, *Journal of Computational and Applied Research in Mechanical Engineering (JCARME)*, Vol. 7, No. 10, pp. 199-207, (2018).
- [23] M. Yadegari and M. Jahangiri, “Simulation of non-Uniform Magnetic Field Impact on non-Newtonian and Pulsatile Blood Flow”, *Journal of Advanced Research in Fluid Mechanics and Thermal Sciences*, Vol. 57, No. 1, pp. 86-99, (2019).
- [24] B. Liu and D. Tang, “Influence of distal stenosis on blood flow through coronary serial stenosis: A numerical study”, *International Journal of Computational Methods*, Vol. 16, No. 3, pp. 1-11, (2019).
- [25] H. C. Han, J. K. Chesnutt, J. R. Garcia, Q. Liu and Q. Wen, “Artery buckling: new phenotypes, models, and applications”, *Annals of biomedical engineering*, Vol. 41, No. 7, pp. 1399-1410, (2013).
- [26] J. M. Downing and D. N. Ku, “Effects of frictional losses and pulsatile flow on the collapse of stenotic arteries”, *Journal of biomechanical engineering*, Vol. 119, No. 3, pp. 317-324, (1997).
- [27] D. Tang, C. Yang, S. Kobayashi and D. N. Ku, “Steady flow and wall compression in stenotic arteries: a three-dimensional thick-wall model with fluid-wall interactions”, *Journal of biomechanical engineering*, Vol. 123, No. 6, pp. 548-557, (2001).
- [28] D. N. Ku, “Blood flow in arteries”, *Annual review of fluid mechanics*, Vol. 29, No. 1, pp. 399-434, (1997).
- [29] Q. Liu and H. C. Han, “Mechanical buckling of artery under pulsatile pressure”, *Journal of biomechanics*, Vol. 45, No. 7, pp. 1192-1198, (2012).
- [30] D. N. Ku, B. N. McCord, “Cyclic stress causes rupture of the atherosclerotic plaque cap”, *Circulation*, Vol. 88, No. 4, pp. 254-254, (1993).
- [31] M. S. Lee and C. H. Chen, “Myocardial bridging: an up-to-date review”, *The Journal of invasive cardiology*, Vol. 27, No. 11, pp. 521-521, (2015).
- [32] M. T. Corban, O. Y. Hung, P. Eshtehardi, E. Rasoul-Arzrumly, M. McDaniel, G. Mekonnen, L. H. Timmins, J. Lutz, R. A. Guyton and H. Samady, “Myocardial bridging: contemporary understanding of pathophysiology with implications for diagnostic and therapeutic strategies”, *Journal of the American College of Cardiology*, Vol. 63, No. 22, pp. 2346-2355, (2014).
- [33] E. G. Frantz, G. W. Henry, C. L. Lucas, B. A. Keagy, M. E. Lores, E. Criado, J. I. Ferreira and B. R. Wilcox, “Characteristics of blood flow velocity in the hypertensive canine pulmonary

- artery”, *Ultrasound in Medicine and Biology*, Vol. 12, No. 5, pp. 379-385, (1986).
- [34] I. V. Pivkin, P. D. Richardson and G. Karniadakis, “Blood flow velocity effects and role of activation delay time on growth and form of platelet thrombi”, *Proceedings of the National Academy of Sciences*, Vol. 103, No. 46, pp. 17164-17169, (2006).
- [35] M. Tomaszewski and J. Małachowski, “Numerical Analysis of the Blood Flow in an Artery with Stenosis”, *International Conference of the Polish Society of Biomechanics*, Cham, pp. 68-77, (2018).
- [36] K. P. Ivanov, M. K. Kalinina and Y. I. Levkovich, “Blood flow velocity in capillaries of brain and muscles and its physiological significance”, *Microvascular research*, Vol. 22, No. 2, pp.143-155, (1981).
- [37] P. D. Richardson, “Effect of blood flow velocity on growth rate of platelet thrombi”, *Nature*, Vol. 245, No. 5420, pp. 103-104, (1973).
- [38] M. Schoenhagen, *Current Developments in Atherosclerosis Research*, Nova Publishers, (2005).
- [39] R. Ross and L. Agius, “The process of atherogenesis-cellular and molecular interaction: from experimental animal models to humans”, *Diabetologia*, Vol. 35, No. 2, pp. S34-S40, (1992).
- [40] Medical Definition of Atherogenesis, <https://www.medicinenet.com/script/main/art.asp?articlekey=24782>, Available: 26.07.2018.
- [41] J. Kolínský, L. Nováková and J. Adamec, “Pressure drop across a double stenosis”, *AIP Conference Proceedings*, Vol. 1768, No. 1. (2016).
- [42] H. Arvidsson, J. Karnell and T. Moller, “Multiple stenosis of the pulmonary arteries associated with pulmonary hypertension, diagnosed by selective angiocardiography”, *Acta radiologica*, Vol. 44, No. 3, pp. 209-216, (1955).
- [43] Q. Zhang, B. Gao and Y. Chang, “Helical Flow Component of Left Ventricular Assist Devices (LVADs) Outflow Improves Aortic Hemodynamic States”, *Medical science monitor: international medical journal of experimental and clinical research*, Vol. 24, pp. 869-879, (2018).
- [44] J. V. Oulis, O. P. Lampri, D. K. Fytanidis and G. D. Giannoglou, “Relative residence time and oscillatory shear index of non-Newtonian flow models in aorta”, *10th International Workshop on Biomedical Engineering, IEEE*, pp. 1-4, (2011).
- [45] M. Jahangiri, M. Saghafian and M. R. Sadeghi, “Numerical simulation of non-Newtonian models effect on hemodynamic factors of pulsatile blood flow in elastic stenosed artery”, *Journal of Mechanical Science and Technology*, Vol. 31, No. 2, pp. 1003-1013, (2017).
- [46] D. De Wilde, B. Trachet, G. De Meyer and P. Segers, “The influence of anesthesia and fluid-structure interaction on simulated shear stress patterns in the carotid bifurcation of mice”, *Journal of biomechanics*, Vol. 49, No. 13, pp. 2741-2747, (2016).
- [47] F. M. Box, R. J. van der Geest, M. C. Rutten and J. H. Reiber, “The influence of flow, vessel diameter, and non-Newtonian blood viscosity on the wall shear stress in a carotid bifurcation model for unsteady flow”, *Investigative radiology*, Vol. 40, No. 5, pp. 277-294, (2005).
- [48] D. N. Ku, D. P. Giddens, C. K. Zarins and S. Glagov, “Pulsatile flow and atherosclerosis in the human carotid bifurcation. Positive correlation between plaque location and low oscillating shear stress”, *Arteriosclerosis: An Official Journal of the American Heart Association, Inc.*, Vol. 5, No. 3, pp. 293-302, (1985).
- [49] A. M. Malek, S. L. Alper and S. Izumo, “Hemodynamic shear stress and its role in atherosclerosis”, *Jama*, Vol. 282, No. 21, pp. 2035-2042, (1999).
- [50] J. Moradicheghamahi, J. Sadeghiseraji and M. Jahangiri, “Numerical solution of the Pulsatile, non-Newtonian and

- turbulent blood flow in a patient specific elastic carotid artery”, *International Journal of Mechanical Sciences*, Vol. 150, pp. 393-403, (2019).
- [51] S. Z. Zhao, X. Y. Xu, A. D. Hughes, S. A. Thom, AV Stanton, B Ariff and Q Long, “Blood flow and vessel mechanics in a physiologically realistic model of a human carotid arterial bifurcation”, *Journal of biomechanics*, Vol. 33, No. 8, pp. 975-984, (2000).
- [52] N. A. Buchmann and M. C. Jermy, “Blood flow measurements in idealised and patient specific models of the human carotid artery”, *Proceedings of the 14th International Symposium on Applications of Laser Techniques to Fluid Mechanics*, Lisbon, Portugal, pp. 7-10, (2008).
- [53] M. O. Khan, K. Valen-Sendstad and D. A. Steinman, “Direct numerical simulation of laminar-turbulent transition in a non-axisymmetric stenosis model for Newtonian vs. shear-thinning non-Newtonian rheologies”, *Flow, Turbulence and Combustion*, Vol. 102, No. 1, pp. 43-72, (2019).
- [54] F. Khalili, P. T. Gamage and H. Mansy, “Prediction of turbulent shear stresses through dysfunctional bileaflet mechanical heart valves using computational fluid dynamics”, *arXiv preprint*, arXiv:1803.03361, pp. 1-9, (2018).
- [55] F. Khalili, P. T. Gamage and H. Mansy, “The Influence of the Aortic Root Geometry on Flow Characteristics of a Bileaflet Mechanical Heart Valve”, *arXiv preprint*, arXiv:1803.03362, pp. 1-7, (2018).

### How to cite this paper:

Bahador Sharifzadeh, Rasool Kalbasi and Mehdi Jahangiri, “The effect of turbulence model on predicting the development and progression of coronary artery atherosclerosis”, *Journal of Computational and Applied Research in Mechanical Engineering*, Vol. 10, No. 1, pp. 183-199, (2020).

**DOI:** 10.22061/jcarme.2019.4628.1561

**URL:** [http://jcarme.sru.ac.ir/?\\_action=showPDF&article=1177](http://jcarme.sru.ac.ir/?_action=showPDF&article=1177)

